Received: 16 June 2022 | Revised: 26 August 2022 | Accepted: 12 September 2022

DOI: 10.1002/jmor.21514

RESEARCH ARTICLE

JOURNAL OF morphology WILEY

Morphometric analysis of the elasmobranch olfactory rosette

Aubrey Clark[1] | Marianne Porter[1] | Tricia Meredith[2]

[1]Department of Biological Sciences, Florida Atlantic University, Boca Raton, Florida, USA

[2]College of Education, Florida Atlantic University, Boca Raton, Florida, USA

Correspondence
Aubrey Clark, Department of Biological Sciences, Florida Atlantic University, Boca Raton, FL, USA.
Email: clarka2014@fau.edu

Funding information
National Science Foundation

Abstract

The olfactory rosettes of elasmobranchs vary in shape and structure among species, but the functional consequences of this diversity are unresolved. Our goal was to quantify rosette morphology on dissected as well as diffusible iodine-based contrast-enhanced computed tomography (diceCT)-imaged specimens to analyze the drivers of observed trends in a phylogenetic context and compare the methodologies. We hypothesized that lamellar count and rosette shape (fineness ratio) would not scale with animal size, but other rosette size variables would scale positively. We dissected rosettes from 14 elasmobranch species and collected morphometric data (fineness ratio, lamellar count, interlamellar distance, lamellar thickness, and raphe width). A subset of rosettes (five species) was used to analyze the effects of body size, while all 14 species were used for a phylogenetic principal component analysis (pPCA). We found that fineness ratio and lamellar counts varied significantly among species, and were positively correlated. The first two principal components of the pPCA explained 82% of the variation, with fineness ratio and lamellar count contributing most to the loadings, respectively. DiceCT was used for in situ imaging of four species of Carcharhiniformes. There were no significant differences between rosette structure or volume when comparing values from dissected specimens to values from in situ specimens obtained using diceCT. We also quantified the volume of the excurrent channel in the olfactory capsule. These data add to our understanding of how olfactory organ shape varies among species and can be used to create three-dimensional models for future olfactory hydrodynamic studies.

KEYWORDS
diceCT, fineness ratio, lamellae, phylogeny, sharks

1 | INTRODUCTION

Olfaction is a sensory modality that fish use to find prey, mates, communicate with conspecifics, and avoid predators (Kleereko-per, 1969). The peripheral olfactory system of fish is generally characterized by a multi-lamellar olfactory organ, or "rosette," overlain with non-sensory and sensory epithelial tissue, with the sensory tissue responding to distinct odor molecules in an aquatic environment (Hansen & Zielinski, 2005; Hara, 1975). Despite these general similarities across elasmobranch species, shape and structure of the olfactory organs vary interspecifically, and the functional implications of these variations are of interest, especially in elasmobranchs because of their perceived status as "super-smellers" (Meredith & Kajiura, 2010; Schluessel et al., 2008; Yopak et al., 2015).

Olfactory rosette morphology varies substantially among elasmobranch species (Meredith & Kajiura, 2010; Schluessel et al., 2008). An elasmobranch olfactory rosette is composed of nasal mucosa, including the olfactory epithelium, that is folded into primary and secondary lamellae and is centrally supported by the raphe (Zeiske et al.,1987). The number, size, and arrangement of lamellae differ among species, with some lamellae extending perpendicular to the raphe, others arranged in a radial pattern around a central axis, and

FIGURE 1 Olfactory morphology. Ventral view of a lemon shark (*Negaprion brevirostris*) with surface tissues removed to expose an olfactory rosette within the capsule. L, lamellae; N, naris; NF, nasal flap; OC, olfactory capsule; OR, olfactory rosette; R, rosette. Shark image credit: Stephen Kajiura.

some without multiple lamellae (Cox, 2008; Hansen & Zielinski, 2005; Yamamoto, 1982). In the anterior chondrocranium, the rosette anchors to the walls of the olfactory capsule which receives water from the external environment via nasal flaps that create incurrent and excurrent nares (Carrier et al., 2012; Ferrando et al., 2019; Timm & Fish, 2012; Figure 1). Water flows into the olfactory capsule via the incurrent naris, over the olfactory lamellae, and back out via the excurrent naris (Abel et al., 2010; Agbesi et al., 2016; Rygg et al., 2013). The fluid dynamics are hypothesized to vary among species due to differing morphologies of the chondrocranium (cartilaginous element surrounding the brain and sense organs), nasal structures, and olfactory organs (Abel et al., 2010; Rygg et al., 2013; Timm & Fish, 2012).

Studies have investigated potential reasons for interspecific variation. Researchers have not been able to correlate organ size and complexity to odor sensitivity in teleosts nor elasmobranchs, indicating that rosette size may not be a good proxy for odor detection abilities (Camilieri-Asch, Yopak, et al., 2020; Hansen & Zielinski, 2005; Meredith & Kajiura, 2010). While a potential relationship between size of teleosts and the number of olfactory lamellae, this has not been found in elasmobranchs and rosette size was shown to be positively correlated with body size (Ferrando et al., 2017; Pashchenko & Kasumyan, 2017; Schluessel et al., 2010; Theiss et al., 2009). Variations in lamellar surface area and lamellar counts were found to be influenced by the selective pressures of life history traits and habitat use, potentially obscuring similarities expected from phylogenetic relationships (Ferrando et al., 2019; Schluessel et al., 2008; Theiss et al., 2009).

In the existing olfactory morphology literature, rosette shape has not been fully explored, whereas rosette size, lamellar number, and lamellar surface area have been quantified for multiple species of elasmobranch (Ferrando et al., 2017, 2019; Meredith & Kajiura, 2010; Schluessel et al., 2008, 2010). While these are important variables, the shape of this organ is likely to have a crucial role in explaining interspecific differences, as it is likely a prime driver of internal flow patterns. Nasal hydrodynamics have been described in an elongated hammerhead rosette (*Sphyrna tudes*), with hypotheses that flow through the olfactory cavity and rosette, influenced by the nasal morphology, could confer a sensory advantage over other species (Kajiura et al., 2005; Rygg et al., 2013). Hammerheads (family Sphyrnidae) are atypical, however, because they have unique external nasal and rosette morphology and these findings may not be representative of other elasmobranch species (Abel et al., 2010; Rygg et al., 2013). Though previous research did not quantify rosette shape, the authors found that water flow is partially determined by external morphology such as nares and grooves (Abel et al., 2010; Rygg et al., 2013). A separate study did measure length and width of the olfactory cavity, but not rosettes or the corresponding internal morphometric variables (Timm & Fish, 2012). We hypothesize that the variable shape of these organs is likely to impact the hydrodynamics of olfaction and influence odorant detection, due to the shared location of the incurrent and excurrent nares at one end of the capsule (Timm & Fish, 2012).

Quantification of olfactory rosette morphology and shape may vary depending on the methods used. The morphology and shape of rosettes is traditionally described using organs that have been dissected from the chondrocranium, causing the rosette to lose the support provided by the olfactory capsule and potentially posing a problem to our understanding of in vivo shape (Ferrando et al., 2017, 2019; Meredith & Kajiura, 2010; Schluessel et al., 2008, 2010). Using methods of in situ visualization, such as X-ray computed tomography (CT), allows for comparison with data from dissected organs, verifying accurate rosette shape quantification.

The goal of this study was to quantify elasmobranch olfactory rosette morphology and shape among species using dissections, phylogenetic comparisons, and diffusible iodine-based contrast-enhanced computed tomography (diceCT) imaging. First, we evaluated olfactory morphology (lamellar count, interlamellar distance, lamellar thickness, and raphe width) and shape (fineness ratio, a two-dimensional [2D] shape metric) for five species over a range of sizes. Previous literature showed that olfactory lamellar count does not change with size, and we hypothesized this would be supported in our study and that rosette 2D shape (fineness ratio) would also be unaffected by animal size (Schluessel et al., 2010). If lamellar count and fineness ratio do not change with animal size, we hypothesized internal rosette size variables must scale with animal growth to retain the rosette shape. Second, we used linear regressions, for variables that did not have significant size effects (fineness ratio and lamellar

TABLE 1 Specimens from superorder Galeomorphi used for rosette morphology statistics

Order	Family	Scientific name	Common name	Number of individuals	Size range (FL, cm)
Lamniformes	Alopiidae	*Alopias vulpinus*	Common thresher shark	10	130–237
	Lamnidae	*Isurus oxyrinchus*	Shortfin mako shark	5	168–233
Carcharhiniformes	Carcharhinidae	*Carcharhinus limbatus*	Blacktip shark	7	38–145
		Rhizoprionodon terraenovae	Atlantic sharpnose shark	5	18–77
	Sphyrnidae	*Sphyrna tiburo*	Bonnethead shark	7	38–70
N =		5		34	

counts), to broadly understand organ morphology effects on shape. We hypothesized that as olfactory lamellar count increases, fineness ratio (length:width) will increase and 2D organ shape will become more rectangular. Third, we examined the impacts of olfactory morphology (four variables) and shape (fineness ratio) in a phylogenetic context using 14 species of elasmobranchs (3 species of Batoidea and 11 of Galeomorphi). We hypothesized that phylogenetic relatedness explains a portion of rosette variation when analyzed using phylogenetic principal component analysis (pPCA). Finally, we used diceCT to compare the methodologies of rosette data collection (*in situ* and dissected organs), and quantified metrics such as excurrent channel volume, raphe width, and incurrent channel diameter.

2 | MATERIALS AND METHODS

2.1 | Olfactory rosette morphology

The ground sharks (Carcharhiniformes) and mackerel sharks (Lamniformes) are sister orders that each contain seven species with varying head morphology, which often impacts olfactory rosette dimensions (Nelson, 2004; Shirai, 1996). Olfactory specimens from species included in this study were received from collaborators collecting for other primary purposes along the eastern coast of the United States. In this study, we examined specimens from orders Carcharhiniformes (3 species; *N* = 19 individuals): bonnethead shark (*Sphyrna tiburo*), blacktip shark (*Carcharhinus limbatus*), Atlantic sharpnose shark (*Rhizoprionodon terraenovae*); and Lamniformes (2 species; *N* = 15 individuals): shortfin mako (*Isurus oxyrinchus*), common thresher shark (*Alopias vulpinus*) (Table 1). Some specimens were received freshly frozen, and they were kept in the freezer until being thawed for dissection and measurement. In addition, we used organs that were previously dissected and stored in a tissue collection.

We measured fork length from the tip of the rostrum to the fork of the caudal fin and olfactory rosettes were dissected from one side of the chondrocranium (Last & Stevens, 2009; *N* = 34 individuals; Table 1). One rosette specimen from each individual was fixed by submerging in 10% phosphate- buffered formalin (Fisher Scientific) for 5–20 days depending on specimen size.

Morphometric data were collected on fixed rosette specimens. Rosettes were removed from formalin, blotted with absorbent paper

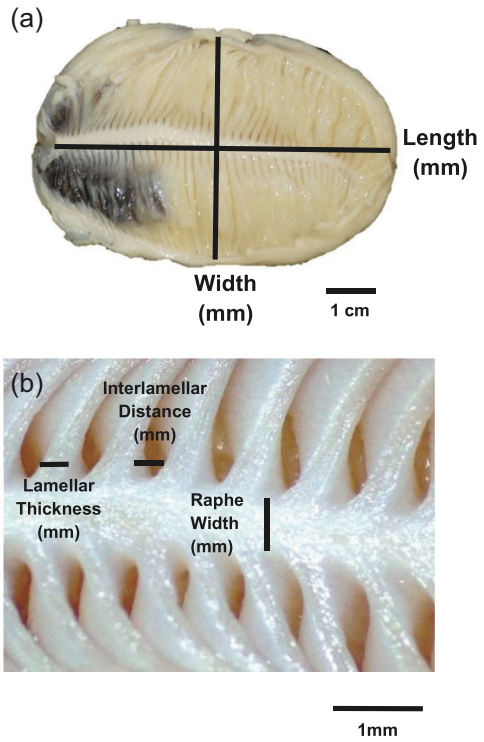

FIGURE 2 Rosette morphometric data collection on blue shark (*Prionace glauca*). Olfactory rosette measurements taken in millimeters (mm). (a) Length measurement was taken from medial to lateral surface. A width measurement was taken at the widest point of the organ, perpendicular to the length. (b) Microscope images were used to measure raphe width, lamellar thickness, and interlamellar distance.

to remove excess fluid, pinned to a dissecting mat, and photographed on a black cloth to minimize glare. Rosettes were pinned to approximate the natural position of the organ in situ, while compensating for potential tissue curling and shrinking during fixation. For each rosette, one photograph was taken using a Nikon D3300 (Melville) camera and measurements were obtained using NIH ImageJ software.

From each photograph, rosette length (mm) was measured from the medial to lateral surface, as a straight line from end to end (Figure 2a). A width measurement (mm) was taken at the widest point (usually near the center; Figure 2a). Fineness ratio, similar to the

aspect ratio of wings, was calculated by dividing the rosette length by the width measurement, giving a unitless value used to evaluate the 2D shape of olfactory rosettes (Vogel, 2013).

Higher magnification images were taken using a Leica EZ4W microscope at three points: 25%, 50%, and 75% along the length of the rosettes, where 50% is at the midpoint of the organ. These three points delineate representative sections that are used to quantify lamellar morphology and are then averaged to give a mean value. To measure the internal rosette morphometrics, we selected three variables. Raphe width (mm) was measured across the raphe at the midpoint of each section, lamellar thickness was taken at the base of one representative lamella (to minimize potential differences in variation along length of lamellae), and the interlamellar distance, defined as the space between the edges of lamellae, was taken at the base of two lamellae (Figure 2b). We took lamellar counts manually, keeping track by using a probe to physically move each lamella being counted.

Data were analyzed using JMP 10 SAS software. When data met ANOVA assumptions, we used mixed model ANOVAs to evaluate the effects of body size, as measured by fork length, species ($N = 5$ species, 4 families, and 2 orders; Table 1), and a body size × species interaction term on the following variables: fineness ratio, lamellar thickness, interlamellar distance, and raphe width. When data were not normal and did not meet ANOVA assumptions, we used a generalized linear model (GLM) to analyze the effects of body size, species, and the interaction term on lamellar count.

2.2 | Phylogenetic principal component analysis

To make phylogenetic comparisons, we used pPCA, which is a method of simplifying complex data into fewer dimensions demonstrating potential trends (Lever et al., 2017). Data are reduced through geometric projections into lower dimensions, referred to as principal components (PC), with the goal of limiting the number of PCs (Lever et al., 2017). Clustering of points can highlight phylogenetic relationships of olfactory rosette morphology and provide potential reasons for variation.

In the morphological analyses above, we only included specimens with known body size (5 species, $N = 34$ individuals). Because body size was not a significant effect in mixed model ANOVAs and GLM examining olfactory rosette morphology, we expanded our survey of specimens in pPCA analyses (7 families, 4 orders, 2 superorders; $N = 59$ individuals, including the previous 34 individuals with known body size; Table 2). We also excluded body size because in PCAs, overall animal size can cause the loading of the first principal component (PC1) to be disproportionately weighted compared to the other variables, leading to an inaccurate explanation of the variance (Björklund, 2019; Bookstein, 1989; Revell, 2009). Five variables (fineness ratio, lamellar count, lamellar thickness, interlamellar distance, and raphe width) were examined. When there was more than one individual per species, prior olfactory morphology pPCA studies have used data from the individual with the largest body size (Ferrando et al., 2019). Because we did not have body size for all individuals, we chose to use the specimen with the largest raphe

TABLE 2 Specimens from superorders Batoidea and Galeomorphi used for pPCA analysis

Order	Family	Scientific name	Common name	Number of individuals
Batoidea				
Myliobatiformes	Myliobatidae	*Rhinoptera bonasus*	Cownose ray	8
Rhinopristiformes	Urolophidae	*Urobatis jamaicensis*	Yellow stingray	3
	Rhinobatidae	*Pseudobatos lentiginosus*	Atlantic guitarfish	2
Galeomorphi				
Lamniformes	Alopiidae	*Alopias vulpinus*	Common thresher shark	10
	Lamnidae	*Isurus oxyrinchus*	Shortfin mako shark	5
Carcharhiniformes	Carcharhinidae	*Carcharhinus limbatus*	Blacktip shark	7
	Sphyrnidae	*Carcharhinus obscurus*	Dusky shark	1
		Carcharhinus plumbeus	Sandbar shark	2
		Negaprion brevirostris	Lemon shark	1
		Prionace glauca	Blue shark	4
		Rhizoprionodon terraenovae	Atlantic sharpnose shark	5
		Sphyrna lewini	Scalloped hammerhead shark	1
		Sphyrna mokarran	Great hammerhead shark	1
		Sphyrna tiburo	Bonnethead shark	9
N =		14		59

width (mm) measurement; and we were able to confirm when possible that this metric scaled with the overall size of the animal.

The phylogenetic tree used in this study was created using the phylogeny with the most inclusive mitochondrial DNA analysis from 595 elasmobranch species (Naylor et al., 2012; Figure 3). Previously established phylogenetic trees were strongly based on morphology and representative species, rather than dense taxonomic DNA evidence (Compagno, 1977; Maisey, 1984). Phylogenetic trees can be represented using the Newick format, that is, an ordered linear form using nested parentheses (Cardona et al., 2008). The Newick tree format used for analysis was:

(((Common_thresher, Shortfin_mako), ((((Blue, Sandbar, Blacktip, Dusky), Lemon), Atlantic_sharpnose), (Great_hammerhead, (Bonnethead, Scalloped_hammerhead)))), (Atlantic_guitarfish, (Yellow_stingray, Cownose_ray))). All branch lengths were set to 1 because we are not including rates of evolution in this study and the length of the branch units does not affect the ordination of the pPCA output (Polly et al., 2012). The tree was loaded into the phytools R-package, which was used to examine the phylogenetic effects among species (Revell, 2012). Using the phyl.pca function, principal component loading values and explanation of variance were calculated.

2.3 | Diffusible iodine-based contrast-enhanced computed tomography

When imaging non-mineralized tissues that do not show up on X-ray well, it is necessary to provide a contrasting agent to increase radiodensity and therefore improve visibility of the resulting scan data (Gignac et al., 2016). Lugol's iodine (I_2KI) is a widely used contrast agent because it is less toxic to handle than other agents, such as osmium tetroxide, and has differential affinities for soft tissue

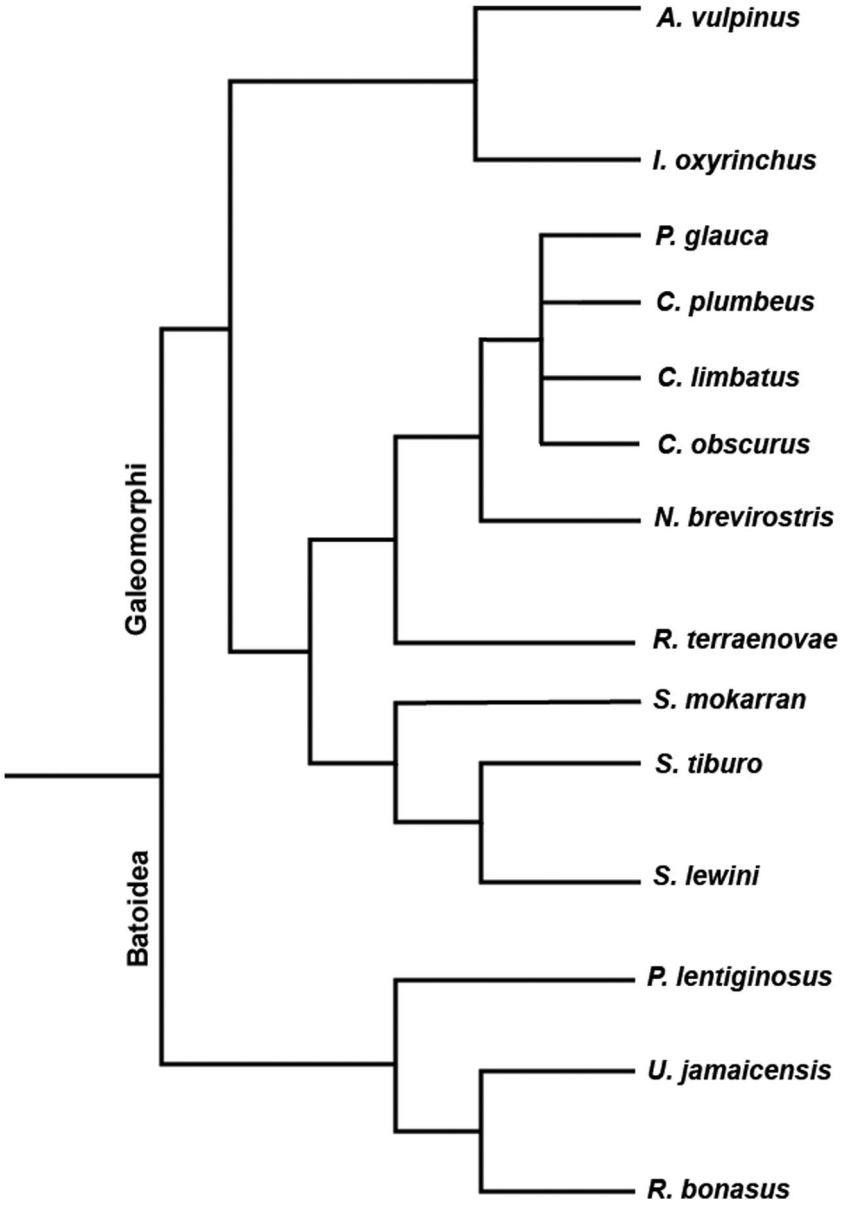

FIGURE 3 Phylogeny of species used for pPCA analysis. A Newick Tree was created to use with phytools R-package (Revell, 2012). Modified from Naylor et al. (2012).

TABLE 3 CT scan olfactory measurements

Species	Fork length (cm)	Excurrent channel volume (mm^3)	Incurrent channel diameter (mm)	Raphe width (mm)
C. plumbeus	113.4	10,197.94	1.02	0.97
C. obscurus	115	5,436.35	1.44	1.08
R. terraenovae	76.5	2,793.71	1.67	1.46
S. tiburo 1	50.2	2,409.53	1.17	0.71
S. tiburo 2	71.5	3,727.37	1.64	0.93
S. tiburo 3	50.2	2,029.35	0.72	0.86
S. tiburo 4	23.7	N/A	0.37	0.33

Note: Excurrent channel volume was not measured for the smallest *S. tiburo* specimen (*S. tiburo* 4; FL- 23.7 cm) due to uncertainty in the distal and medial ends of the olfactory capsule.

(Gignac et al., 2016). DiceCT refers to the use of iodine staining to produce detailed images of soft tissues (Gignac et al., 2016). The unmineralized olfactory rosettes being examined in this study required diceCT for clear visualization.

Species from the order Carcharhiniformes were used for microCT scanning and included a bonnethead shark (*Sphyrna tiburo*, $N = 5$), Atlantic sharpnose shark (*Rhizoprionodon terraenovae*, $N = 1$), sandbar shark (*Carcharhinus plumbeus*, $N = 1$), and dusky shark (*Carcharhinus obscurus*, $N = 1$). Specimens used for diceCT scanning retained one olfactory rosette in situ in the olfactory capsule of the chondrocranium ($N = 4$ species; Table 3). The other rosette was dissected and processed as described in Section 2.1. In specimens too large for the machine (14 cm width × 20 cm length), a head section was taken by removing a transverse slice from the rostral area or by creating a midline cut that retains olfactory organs, to enhance infiltration of solutions and to ensure fit in the microCT scanner (Figure 4). Following a modified protocol from Gignac et al. (2016), each sample was fixed in 10% buffered formalin for 7–14 days. After being fixed in formalin, the specimen was threaded with fishing line and suspended in an opaque bucket with 5% Lugol's Iodine (I_2KI; Fisher Scientific). A shaker table was used to maintain even diffusion of the solution into tissues. After 5 days, specimens were scanned. If the scan did not produce clear images of the soft olfactory tissues, specimens were replaced in the Lugol's solution for two more days. After staining, the specimen was moved into deionized water for one day to remove excess dye before imaging. After a clear scan of olfactory tissues was obtained, de-staining was accomplished with 5% sodium thiosulfate ($Na_2S_2O_3$), enabling these specimens to be stained again using Lugol's Iodine or another staining agent for other studies.

Following modified protocols, each fixed stained specimen was gently blotted dry with gauze and placed in a plastic canister and packed tightly with gauze to prevent movement during scanning (Gignac et al., 2016). We performed microCT imaging with a Bruker Skyscan 1173 scanner at 130 kV (kilovolts), 61 µA (amperage, X-ray intensity), and between 30 and 40 µm pixel size. X-ray slices were used to reconstruct three-dimensional (3D) images using Bruker NRecon and CTVox software. Scans were segmented using Bruker DataViewer software to determine the optimal positioning for the olfactory capsule and rosette analysis. The scans were loaded into Bruker CTAn software to create a 3D model and analyze 3D measurements. Rosette length and width were measured and fineness ratio was calculated (L/W). Regions of interest (ROI) were selected for the olfactory capsule and rosette using Bruker CTAn. The excurrent channel space in the capsule was also quantified.

To determine the effects of the quantification method on rosette measurements, fineness ratio and volume data measured or calculated from dissected organs and from in situ CT scanned specimens were analyzed using Welch's *t*-tests (Taeger & Kuhnt, 2014). For each dissected organ, we measured olfactory rosette volume (ml) through water displacement in a graduated cylinder to the nearest 0.1 ml. Containers were gently tapped to remove any visible air bubbles. For CT scans, we measured the volume of the excurrent channel, width of the raphe, and diameter of the incurrent channel. We also analyzed the relationship between incurrent channel diameter and raphe width using a linear regression in JMP 10 SAS software.

3 | RESULTS

3.1 | Olfactory rosette morphology

We aimed to quantify elasmobranch olfactory rosette morphology (raphe width, lamellar thickness, interlamellar distance, and lamellar count) and shape (fineness ratio) for five species over a range of sizes, using organs that were dissected from the chondrocranium.

A mixed model ANOVA examining raphe width (mm) among species and sizes was significant ($F_{9,24} = 11.9201$; $p < .0001$). Neither the main effects (species, animal fork length) nor the interaction term was significant. Mixed model ANOVAs examining lamellar thickness and interlamellar distance were not significant (Table 4).

A mixed model ANOVA examining rosette fineness ratio among species of various sizes was significant ($F_{9,24} = 72.7137$; $p < .001$). Species was a significant main effect ($F_{4,4} = 13.959$; $p < .0001$; Figure 5; Table 5). Tukey LSD *post hoc* comparisons showed that the bonnetheads had significantly larger fineness ratios, and their rosettes were more elongated, than all the other species (Figure 5 and Table 6). The lamniformes (common thresher and shortfin mako) fineness ratios were significantly smaller and more stoutly shaped, than bonnetheads and blacktips, but similar to Atlantic sharpnose. Fork length and the species × fork length interaction terms were not significant.

A generalized linear model (GLM), using a Poisson distribution, examining lamellar counts was significant ($\chi^2_{df=9} = 319.5295$; $p < .0001$). Species was a significant effect ($\chi^2_{df=4} = 36.392771$; $p < .0001$; Figure 6 and Table 5), while fork length and the species × fork length interaction terms were not. Steel-Dwass *post*

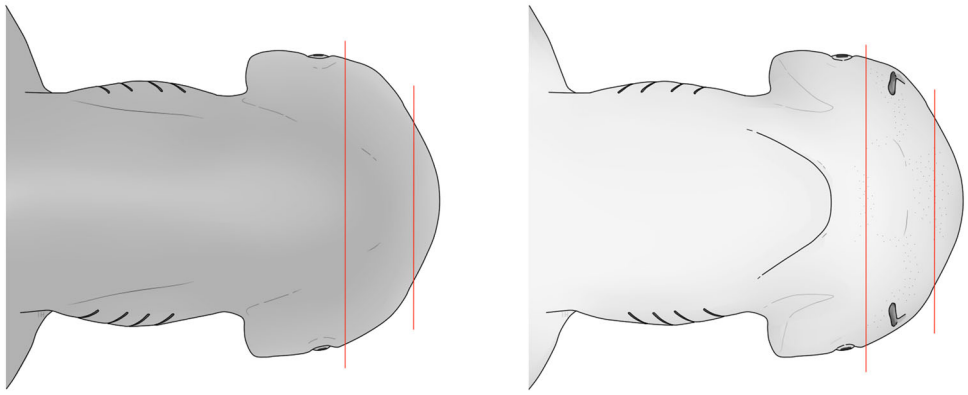

FIGURE 4 DiceCT tissue preparation. (a) Dorsal and (b) ventral view of a bonnethead (*Sphyrna tiburo*) with red lines (1) indicating transverse slices made to the head and blue lines (2) demonstrating an alternative dissection method. The resulting section retains at least one olfactory rosette and capsule. Image credit: I. Heerdegen.

TABLE 4 Descriptive statistics for nonsignificant variables

	Interlamellar distance (μm)			Lamellar thickness (mm)		
Species	**Mean**	***SE***	***SD***	**Mean**	***SE***	***SD***
A. vulpinus	240	10	30	0.46	0.03	0.11
I. oxyrinchus	250	20	50	0.39	0.03	0.07
C. limbatus	370	90	250	0.71	0.20	0.52
R. terraenovae	120	10	30	0.21	0.07	0.15
S. tiburo	270	30	80	0.32	0.02	0.04

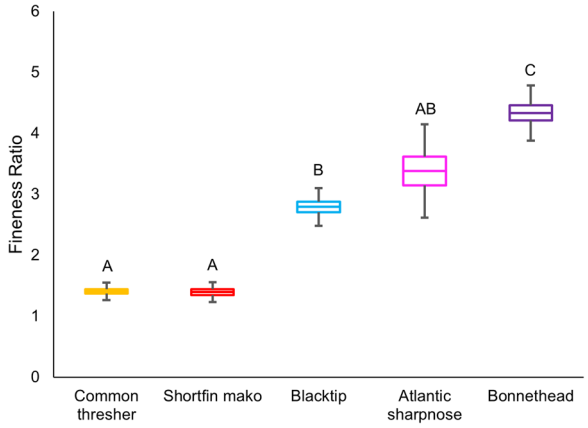

FIGURE 5 Fineness ratio varied significantly with species ($p < .0001$). The center bar in each box denotes the mean, boxes are means ± standard errors, and whiskers are *SD*s. Boxes sharing the same letter are statistically similar, according to Tukey LSD *post hoc*.

hoc comparisons showed that bonnethead lamellar counts were significantly greater than common thresher ($Z = 3.373$; $p = .0067$), blacktip ($Z = 3.073$; $p = .018$); shortfin mako ($Z = 2.771$; $p = .044$), and Atlantic sharpnose ($Z = 2.775$; $p = .0438$; Figure 6). Blacktip lamellar counts were significantly greater than common thresher ($Z = 3.373$; $p = .0067$), shortfin mako ($Z = -2.77$; $p = .044$), and Atlantic sharpnose ($Z = -2.775$; $p = .0438$). Common thresher lamellar counts were significantly greater than shortfin mako ($Z = -3.01$; $p = .0221$; Table 7).

To examine the relationship between lamellar count on olfactory rosette shape, both of which were variables not impacted by animal size (Figures 5 and 6), we used a linear regression from the five species examined above and nine additional species for which we did not have fork length measures (Table 2). For species with more than one individual representative, we calculated mean fineness ratio and mean lamellar count to create one value to avoid pseudoreplication. We found that as the fineness ratio increases among species and rosettes become more rectangular, the number of lamellae also increases significantly ($F_{1,12} = 17.238$; $p = .0013$; $R^2 = 0.59$; Figure 7). For example, as fineness ratio doubles (2–4), lamellae count will also double (100–200).

3.2 | Phylogenetic principal component analysis

The pPCA utilized data from the specimens in Table 2. The first two principal components (PC1 and PC2) explained 82.1% of the pPCA variation (45.3% and 36.8%, respectively; Figure 8 and Table 8). Loadings of PC1 and PC2 were analyzed to determine the

TABLE 5 Mixed model ANOVAs and GLM showing differences among species and over a range of sizes (fork length, FL)

		Fineness ratio			Lamellar count			Raphe width (mm)		
		F	*df*	*p*	X^2	*df*	*p*	*F*	*df*	*p*
Whole model		**72.7**	**9,24**	**<.0001**	**319.5**	**9**	**<.0001**	**11.9**	**9,24**	**<.0001**
Effects test	Species		<.0001		36.4	4	<.0001		NS	
	Fork		NS			NS			NS	
	Length									
	Species × FL		NS			NS			NS	

TABLE 6 Descriptive statistics and *post hoc* comparisons for significant variables

	Fineness ratio				Lamellar count				Raphe width (mm)			
Species	**Mean**	***SE***	***SD***	***Tukey***	**Mean**	***SE***	***SD***	**St-Dw**	**Mean**	***SE***	***SD***	***Tukey***
A. vulpinus	1.41	0.03	0.11	A	71.2	1.94	6.12	A	2.53	0.17	0.54	A
I. oxyrinchus	1.39	0.05	0.11	A	51.2	1.02	2.28	B	2.32	0.18	0.40	A
C. limbatus	2.79	0.08	0.22	B	107	1.36	3.61	C	1.16	0.33	0.87	A
R. terraenovae	3.38	0.24	0.53	AB	81.6	3.66	8.17	AB	0.35	0.05	0.12	A
S. tiburo	4.33	0.12	0.33	C	137.57	1.90	5.03	D	0.35	0.01	0.03	A

Note: Tukey LSD *post hoc* analysis was used for fineness ratio and raphe width. Steel-Dwass, a nonparametric *post hoc* analysis, was used for lamellar count.

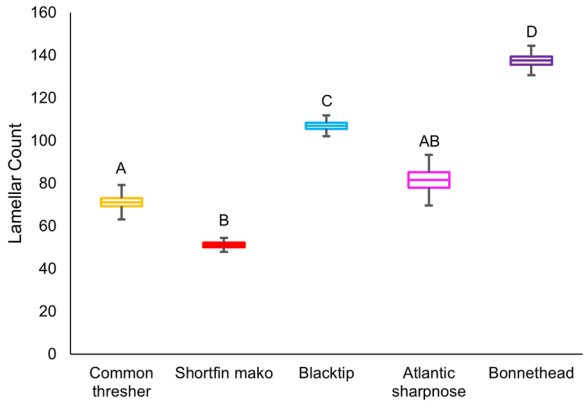

FIGURE 6 Lamellar count varied significantly with species ($p < .0001$). The center bar in each box denotes the mean, boxes are means ± *SE*, and whiskers are *SD*s. Boxes sharing the same letter are statistically similar, according to Steel-Dwass *post hoc* (Table 7).

TABLE 7 Descriptive *post hoc* (Steel-Dwass) statistics for lamellar count GLM

Level	Level	*Z*	*p* Value
C. limbatus	*A. vulpinus*	3.3731	.0067
S. tiburo	*A. vulpinus*	3.3731	.0067
S. tiburo	*C. limbatus*	3.0734	.0180
S. tiburo	*I. oxyrinchus*	2.7705	.0444
S. tiburo	*R. terraenovae*	2.7754	.0438
R. terraenovae	*A. vulpinus*	2.0914	.2237
R. terraenovae	*I. oxyrinchus*	2.5298	.0841
I. oxyrinchus	*C. limbatus*	−2.7705	.0444
R. terraenovae	*C. limbatus*	−2.7754	.0438
I. oxyrinchus	*A. vulpinus*	−3.0087	.0221

relationship among variables (Table 9). PC1 positively correlated with fineness ratio and negatively correlated with lamellar thickness (mm) (Table 9). PC2 did not positively correlate with any of the tested variables; there was a strong negative correlation with lamellar count.

3.3 | DiceCT

Olfactory rosettes were clearly visible on the microCT scan images after staining for 5 or 7 days in 5% Lugol's iodine (Figure 9). Using a Welch's *t*-test, we compared the mean rosette volume (mm^3) for dissected and in situ organs (mm^3) and found no significant difference (N = 6; $p = .9405$; Table 10). To examine the shape effects of removing the rosette from the olfactory capsule, we compared fineness ratios from dissected organs and those imaged using CT scans using Welch's *t*-test. There was not a significant difference in the mean fineness ratio between quantification methods ($N = 6$; $p = .512$; Table 10).

During dissections and CT scan analysis, we noted the presence of the incurrent and excurrent channels previously described in the literature (Abel et al., 2010; Rygg et al., 2013). We quantified the volume of the excurrent channel from CT scans for the four species examined here (Table 3). We also measured the diameter of the incurrent channel and width of the raphe at a

central location on the rosette because these areas were unclear at the distal and medial ends (Table 3). We found that raphe width significantly scaled with the diameter of the incurrent channel (p = .0282; Figure 10).

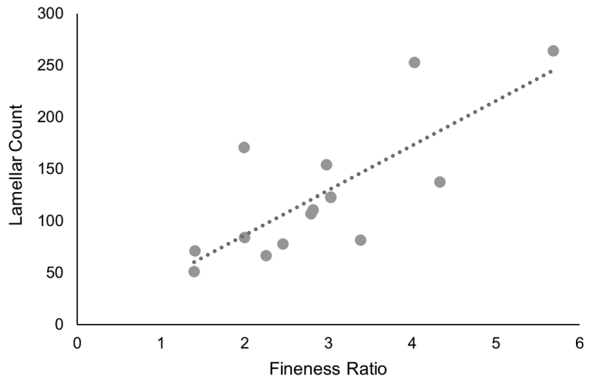

FIGURE 7 Lamellar count varied significantly with fineness ratio ($F_{1,12}$ = 17.238; p = .0013; R^2 = 0.59). A more rectangular rosette (extending lengthwise orthogonal to the long axis of the body) will have more lamellae than a squarer rosette. Data points correspond to species in Table 2.

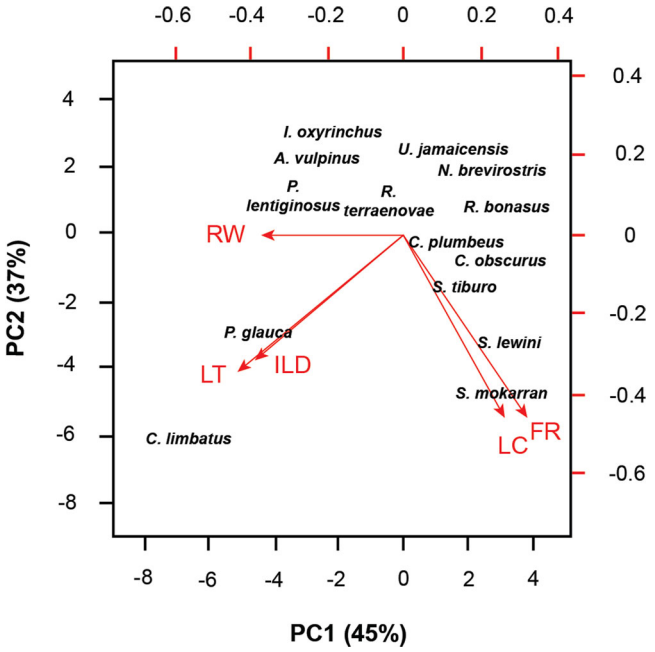

FIGURE 8 pPCA analysis. PC1 explains 47% of variation while PC2 explains 31% of variation (N = 14 species). Species correspond to Table 2. FR, fineness ratio, ILD, interlamellar distance, LC, lamellar count; LT, lamellar thickness; RW, raphe width.

4 | DISCUSSION

Though elasmobranchs possess multiple sensory systems, olfaction certainly plays an important role in their ability to survive and find resources including food and mates (Schluessel et al., 2008; Yopak et al., 2015). Variations within the olfactory system of these species have been documented in the literature; however, the functional consequences for these variations are not fully understood (Ferrando et al., 2017; Meredith & Kajiura, 2010; Meredith et al., 2012; Schluessel et al., 2008; Yopak et al., 2015). Organ size is hypothesized to be correlated with sensitivity and morphological variations among species' olfactory systems are hypothesized to result from phylogeny, habitat, or flow optimization (Ferrando et al., 2019; Kajiura et al., 2005; Schluessel et al., 2008; Theisen et al., 1986; Timm & Fish, 2012).

Here, we quantified olfactory rosette morphology and shape among a diverse set of elasmobranch species. To our knowledge, this study is the first to quantify rosette shape using fineness ratio and utilize internal morphometric data (interlamellar distance, lamellar thickness, and raphe width) over a range of sizes in a phylogenetic context (Figures 5–8). We found that body size did not significantly impact any rosette variables in our study (N = 5 species, 34 individuals), but fineness ratio and lamellar count did vary among species (Figures 5 and 6). When considering overall trends in rosette structure, we found that lamellar count increased significantly with fineness ratio (Figure 7).

Phylogenetic analyses showed that fineness ratio and lamellar count contributed most to the loadings of the two principal components, respectively (Table 8). We also used in situ values of rosette volume and fineness ratio from diceCT to assess the impacts of dissection on morphological measurements. Rosette measurements from dissected organs did not differ significantly compared to those from CT scans, supporting the validity of both methods (Table 10).

TABLE 9 PCA loadings of principal component 1 (PC1) and principal component 2 (PC2)

	PC1	PC2
Fineness ratio	0.5910	−0.7612
Lamellar count	0.5071	−0.8005
Lamellar thickness (mm)	−0.7891	−0.5806
Interlamellar distance (mm)	−0.7465	−0.5321
Raphe width (mm)	−0.6921	−0.0005

TABLE 8 Explanation of principal component variance

	PC1	PC2	PC3	PC4	PC5
SD	1.5051688	1.3566266	0.8422944	0.3864128	0.1877669
Proportion of variance	0.4531066	0.3680872	0.1418920	0.0298629	0.0070512

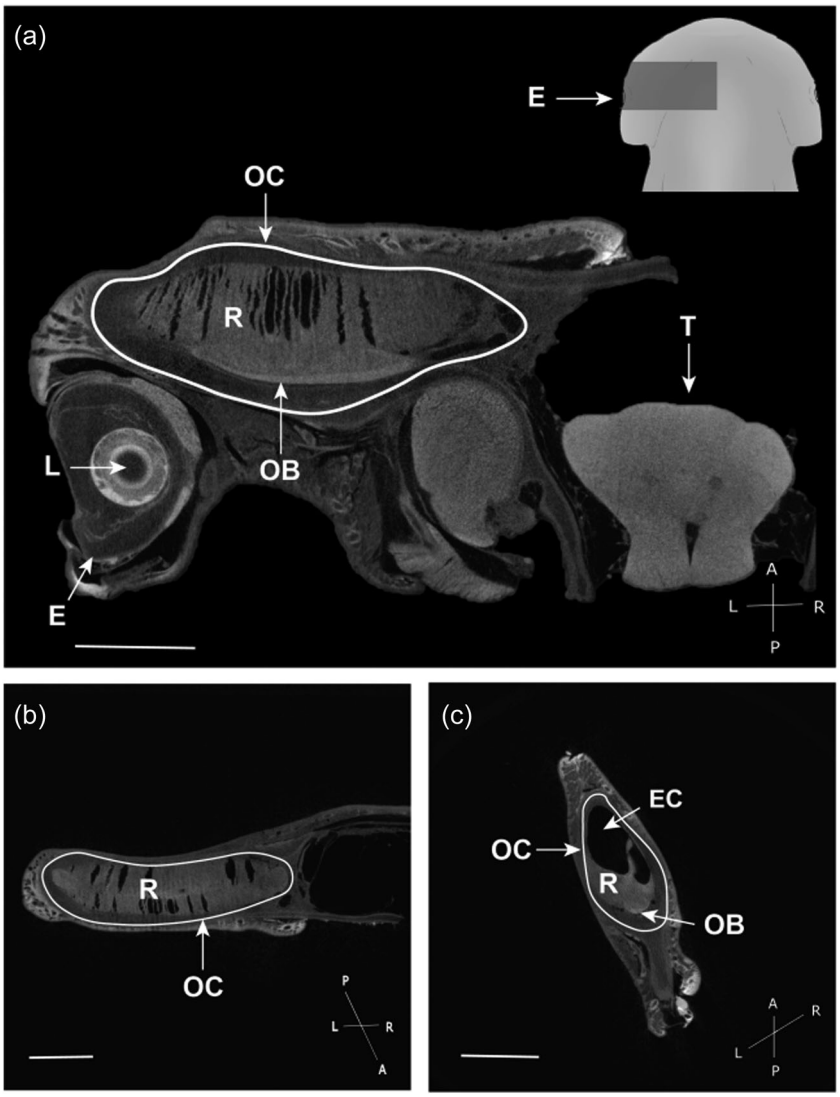

FIGURE 9 Bonnethead (*S. tiburo*) imaged using diceCT. (a) Image taken in coronal plane showing rosette within the capsule. Dorsal view of head in upper right corner. (b) Transverse plane image with rosette and empty space in capsule. (c) Sagittal plane image. Right portion of the olfactory system has been removed for morphological data collection. E, eye; EC, excurrent channel; L, lens; OB, olfactory bulb; OC, olfactory capsule; R, rosette; T, telencephalon. All scale bars are 1 cm.

TABLE 10 CT morphological comparisons using Welch's *t*-test

	Mean	*SD*	*t*	*df*	*p*
Rosette FR	3.50	0.74	0.69	7.50	.51
CT Rosette FR	4.00	1.43			
Rosette volume (mm^3)	2483.33	1664.23	−0.08	6.97	.94
CT Rosette volume (mm^3)	2425.61	754.35			

Abbreviation: FR, fineness ratio.

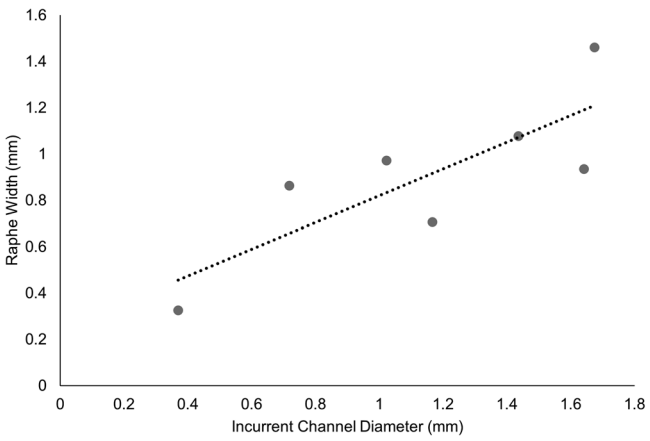

FIGURE 10 Raphe width scaled significantly within current channel diameter ($F_{1,5} = 9.3491$, $p = .0282$, $R^2 = 0.6515$). Data points correspond to Table 3.

4.1 | Olfactory rosette morphology

Overall, we found that bonnethead shark (*S. tiburo*) rosettes can be characterized as elongated and extending lengthwise orthogonal to the long axis of the body, with a thin raphe, and many, closely-spaced lamellae (Tables 4 and 6). Though not quantified, previous studies

have noted long thin olfactory organs in other members of the hammerhead family (Sphyrnidae; Abel et al., 2010; Kajiura et al., 2005; Rygg et al., 2013). Common thresher sharks (*A. vulpinus*) and shortfin mako sharks (*I. oxyrinchus*), from the order Lamniformes, share similarities in their rosettes: a shape that is almost as wide as it is long, a thicker raphe, fewer lamellae, and wider interlamellar distances. Blacktip sharks (*C. limbatus*) and Atlantic sharpnose sharks (*R. terraenovae*), both in the family Carcharhinidae (requiem sharks), have rosettes that are intermediate to the two aforementioned groups.

When we included phylogeny in our analyses of the rosette's shape and morphology, we found that the pPCA data were compressed into two principal components that explained 82% of the total variation, supporting our hypothesis that phylogeny accounts for a portion of rosette variation (Figure 8). PC1 was positively correlated with fineness ratio and negatively correlated with lamellar thickness. PC2 was most negatively correlated with lamellar count (Table 9). The loadings of these components indicate that rosette shape is critical for understanding the variation that exists in phylogenetically distinct species. In order Carcharhiniformes (superorder Galeomorphi), members of family Sphyrnidae are clustered, while the species of family Carcharhinidae are spread over a larger area. The two species of order Lamniformes are aggregated, without overlapping the Carcharhiniformes. Members of superorder Batoidea are located intermediate to the two Galeomorphi orders (Figure 8). The location of these superorders is consistent with the results found in a previous study examining secondary lamellar folding (Ferrando et al., 2019). Our results and the scope of the study would be strengthened through the inclusion of more Elasmobranchii orders.

Elasmobranch and teleost olfactory systems are morphologically similar and are frequently compared (Ferrando et al., 2017; Meredith & Kajiura, 2010; Theisen et al., 1986; Theiss et al., 2009; Yopak et al., 2015). It has been shown in teleosts that the structure of the olfactory organs, amount of primary folding of the epithelium, and size of the organs varies among species (Hansen & Zielinski, 2005; Schluessel et al., 2010). Age can also affect the amount of folding that is seen in some teleost species, with more lamellae in older individuals (Hansen & Zielinski, 2005). Schluessel et al. (2010) found that this was not true for elasmobranchs—the number of lamellae remained relatively constant throughout growth of the species examined. The results of our study support previous research because body size was not a significant effect in our lamellar count or fineness ratio statistical models. We hypothesized that these variables would remain constant because there are not significant chondrocranium alterations throughout ontogeny (Irschick & Hammerschlag, 2015; Irschick et al., 2017). Fully developed organs at a young age may also indicate that olfaction is an important sensory modality throughout all life stages. Species was a significant effect for both models examining lamellar count and fineness ratio over a range of body sizes (Figures 5 and 6), supporting the interspecific differences found in previous studies (Meredith & Kajiura, 2010; Schluessel et al., 2008).

We also hypothesized that internal rosette dimensions (interlamellar distance, lamellar thickness, and raphe width) would scale proportionally (isometrically) with overall body growth because they are constrained by consistent rosette shape and number of lamellae. Our results did not support this hypothesis. Previous research found that rosette size was positively correlated with body mass and length, and only two species scaled isometrically whereas the others (N = 5 species) scaled with less than proportional allometric growth (Schluessel et al., 2010). Raphe width was significant but none of the main effects in the statistical model were significant (Table 5). The models for lamellar thickness and interlamellar distance were not significant. Though our data set included five species and at least five individuals per species, we were not able to capture olfactory morphology over the entire size range of each species. Specimens used in this study were regionally available and collected post-mortem, which limited the number of individuals that we were able to include in analyses with body size (fork length). A full spectrum of ontogenetic development, from embryo to large adult, would provide a better understanding of the effects of body size on these internal dimensions.

To broadly examine patterns in rosette shape and internal structure, we quantified the relationship between fineness ratio and lamellar count for 14 species. We found that as the fineness ratio increased, the lamellar number also increased (Figure 7). A longer and narrower rosette, such as those seen in family Sphyrnidae, will have more lamellae than a rosette that is shorter and wider, like in a common thresher shark (Table 4). This correlation suggests that the number of lamellae and organ shape are related and may work in conjunction to direct water flow throughout the system (Timm & Fish, 2012). Previous hypotheses suggested that olfactory rosette size is correlated to organ sensitivity, perpetuating the idea that sharks are "swimming noses" (Aronson, 1963; Northcutt 1978; Yopak et al., 2015). However, experimental data showed that olfactory morphology did not correlate with sensitivity by measuring physiological responses of the olfactory epithelium to amino acids and bile salts using the underwater electro-olfactogram technique (EOG; Meredith & Kajiura, 2010; Meredith et al., 2012). Species, such as hammerheads (Sphyrnids), have more lamellae compared to species with elongated rostra (Carcharhinids), and one previous study showed no differences in the olfactory thresholds (Meredith & Kajiura, 2010). Interpretations of some of these studies have limitations because they used one flow rate, which was estimated from the nasal morphology and swimming speed of scalloped hammerhead sharks, regardless of the lamellar number measured or external morphology for other species (Meredith & Kajiura, 2010; Meredith et al., 2012; Tricas et al., 2009). Previous research suggests that the number of lamellae is not a predictor of odorant sensitivity, and we hypothesize that it may have impacts on odor detection when considered in the context of overall rosette shape and water flow.

4.2 | Hydrodynamic implications

The olfactory hydrodynamics of elasmobranchs is an expanding field with a few notable studies paving the way (Abel et al., 2010; Agbesi et al., 2016; Rygg et al., 2013; Timm & Fish, 2012). Though we do not

have extensive olfactory data for a broad range of elasmobranchs, we can look to a similarly structured system, the gills of teleost fishes, to understand potential hydrodynamic behavior in lamellar structures. In the respiratory tract, water flows through secondary lamellae of the gills, plate-like structures similar to the lamellae of an olfactory rosette, that are comparable in arrangement and also bind to dissolved chemicals in the water (Grigg, 1970; Strother, 2013a). Studies have examined gill tissue to determine the hydrodynamic resistance across gills and to characterize the flow patterns among lamellae, including the secondary lamellae, using excised gills and computational fluid dynamics (CFD; Strother, 2013a, 2013b). An increase in gill lamellar thickness led to small decreases in the amount of flow volume passing through the interlamellar channel instead of between the tips of the secondary lamellae (Strother, 2013b). Olfactory rosettes also demonstrate secondary folding on their lamellae that significantly increase the surface area (Ferrando et al., 2019). They also found that as gill interlamellar distance decreased, flow velocities were greatest in between the tips of the secondary lamellae, while a larger interlamellar distance caused flow velocities to increase and distribute uniformly (Strother, 2013b). A different study investigated lamellar arrangement in gills and determined that optimal interlamellar spacing allows for maximization of oxygen transfer at a certain pressure (Park et al., 2014). While the physiology of olfaction and respiration are different, these data support our hypotheses that rosette shape and structure may have evolved to optimize water flow and odorant detection.

In previous hydrodynamic studies on a hammerhead (*Sphyrna tudes*) specimen, it was assumed that flow in the nasal region, including sensory channels within the rosette, was laminar due to Reynolds numbers obtained at the fastest simulated swimming speeds (Rygg et al., 2013). Based on these findings, we hypothesize that the elasmobranch olfactory system of other species may exhibit similar fluid dynamics and that internal rosette variables, such as lamellar thickness, interlamellar distance, and raphe width, will affect flow patterns and odorant binding (Park et al., 2014; Rygg et al., 2013, Strother, 2013a, 2013b). From five species examined here, we hypothesize that rosette hydrodynamics will vary among orders (Lamniformes and Carcharhiniformes). Most notably the Sphyrnids (bonnethead) have smaller interlamellar distances and greater fineness ratios, which may lead to higher flow velocities at the tips of the lamellae and putative stagnation zones at the distal ends of the rosettes (Tables 4 and 6). In contrast, the lamniforms may have a more even flow distribution throughout the rosette due to the larger distances between the lamellae and smaller fineness ratio (Tables 4 and 6). Because the lamniforms have thicker lamellae, they may also experience a decrease in the amount of water that flows through the channels between the lamellae. Future studies should investigate these hypotheses with CFD modeling.

4.3 | DiceCT

An accurate characterization of rosette shape is crucial for understanding variation among species. The most widely used method is measuring organs that have been dissected from the chondrocranium

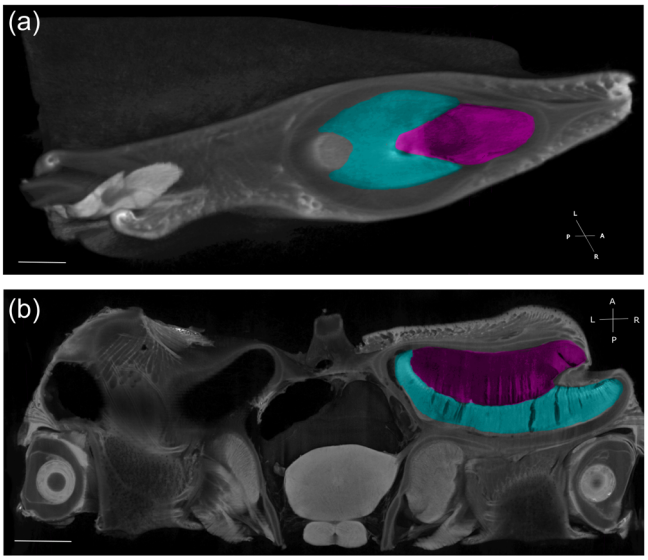

FIGURE 11 Channels in olfactory capsule of bonnethead shark (*S. tiburo*). (a) Sagittal and (b) coronal plane image demonstrating olfactory rosette within the olfactory capsule. Rosette highlighted in aqua and channels highlighted in magenta. All scale bars are 1 cm.

(Ferrando et al., 2017, 2019; Meredith & Kajiura, 2010; Meredith et al., 2012; Yopak et al., 2015; Schluessel et al., 2008). We used this method for Sections 2.1 (rosette morphology) and 2.2 (pPCA) of this study and aimed to compare those measurements to in situ rosette values obtained from CT scans (Section 2.3). We provide support that rosettes are not significantly altered in the traditional data collection protocol. We found that rosette volumes and fineness ratio were not significantly different between the two methods (Table 10).

We measured internal metrics of the olfactory system, including the volume of the excurrent channel (Figures 9 and 11; Table 3). A recent study using diceCT to examine an elasmobranch nervous system reported a shrinkage of 14% for brain tissue in their specimens (*Chiloscyllium punctatum*; Camilieri-Asch, Shaw, et al., 2020). While the diceCT protocol differed from this study, such as choice of fixative and percentage of Lugol's iodine used, their results suggest that the excurrent channel measured could be partially affected by tissue shrinkage during preservation. We also measured raphe width and incurrent channel diameter to determine if raphe width could be used as a proxy for the size of the incurrent channel. These variables significantly scaled and provide preliminary evidence that raphe width should be considered in future hydrodynamic studies, especially when dissected olfactory organs are used and the channel geometry cannot be preserved. These data are also useful for understanding the incurrent channel without having to permanently damage rosettes through dissection.

5 | CONCLUSIONS

Our evaluation of olfactory organ morphology focused on explaining variation via quantification of rosette shape and internal structures. Rosette fineness ratio (shape) and lamellar number

varied among species of elasmobranchs. Overall, there are more lamellae in a rosette with an elongated shape than in an organ with a short and wide shape. Throughout the ontogenetic sampling of our study, we did not see changes in rosettes, though they are expected to scale with body dimensions. Looking at a broad size range of specimens is key to further address this question. The organs also did not change in shape or number of lamellae, suggesting that olfaction is a key sensory modality throughout the life of elasmobranch fishes. The shape and internal structure should be considered when characterizing olfactory rosettes in future studies because fineness ratio and lamellar number were the largest contributors to our phylogenetic analyses. The data collected here should be used to further investigate rosette variation among elasmobranch species by examining the hydrodynamics of the olfactory system with 3D models and quantifying the physiological impacts of flow on odorant binding.

ACKNOWLEDGMENTS

The authors thank Dr. Lisa Natanson (NOAA), Dynasty Marine Associates, and Dr. Stephen Kajiura for providing specimens. The authors are also grateful to the FAU High School Owls Imaging Lab for providing microCT equipment. The authors thank Charles Dante Romero for assisting with dissections and morphometric data collection. The authors also thank Ivan Heerdegen for their illustration in Figure 4. Funding from the National Science Foundation (NSF, IOS-1941713) supported Marianne Porter.

DATA AVAILABILITY STATEMENT

The data that support the findings of this study are available from the corresponding author upon request.

ORCID

Aubrey Clark http://orcid.org/0000-0002-5612-2272

REFERENCES

Abel, R. L., Maclaine, J. S., Cotton, R., Xuan, V. B., Nickels, T. B., Clark, T. H., Wang, Z., & Cox, J. P. L. (2010). Functional morphology of the nasal region of a hammerhead shark. *Comparative Biochemistry and Physiology Part A: Molecular & Integrative Physiology*, *155*(4), 464–475.

Agbesi, M. P. K., Naylor, S., Perkins, E., Borsuk, H. S., Sykes, D., Maclaine, J. S., Wang, Z., & Cox, J. P. L. (2016). Complex flow in the nasal region of guitarfishes. *Comparative Biochemistry and Physiology Part A: Molecular & Integrative Physiology*, *193*, 52–63.

Aronson, L. R. (1963). The central nervous system of sharks and bony fishes with special reference to sensory and integrative mechanisms. In P. W. Gilbert (Ed.), *Sharks and survival* (pp. 165–241). Health.

Björklund, M. (2019). Be careful with your principal components. *Evolution*, *73*(10), 2151–2158.

Bookstein, F. L. (1989). "Size and shape": A comment on semantics. *Systematic Zoology*, *38*(2), 173.

Camilieri-Asch, V., Shaw, J. A., Mehnert, A., Yopak, K. E., Partridge, J. C., & Collin, S. P. (2020). diceCT: A valuable technique to study the nervous system of fish. *eNeuro*, *7*(4), 1–21.

Camilieri-Asch, V., Yopak, K. E., Rea, A., Mitchell, J. D., Partridge, J. C., & Collin, S. P. (2020). Convergence of olfactory inputs within the central nervous system of a cartilaginous and a bony fish: An anatomical indicator of olfactory sensitivity. *Brain Behavior and Evolution*, *95*, 139–161.

Cardona, G., Rosselló, F., & Valiente, G. (2008). Extended Newick: It is time for a standard representation of phylogenetic networks. *BMC Bioinformatics*, *9*(1), 532.

Carrier, C., Musick, J., & Heithaus, M. (2012). *Biology of sharks and their relatives* (2nd ed.). CRC Press.

Compagno, L. J. V. (1977). Phyletic relationships of living sharks and rays. *American Zoologist*, *17*, 303–322.

Cox, J. P. L. (2008). Hydrodynamic aspects of fish olfaction. *Journal of the Royal Society Interface*, *5*(23), 575–593.

Ferrando, S., Amaroli, A., Gallus, L., Aicardi, S., Di Blasi, D., Christiansen, J. S., Vacchi, M., Ghigliotti, L., & Ghigliotti, L. (2019). Secondary folds contribute significantly to the total surface area in the olfactory organ of chondrichthyes. *Frontiers in Physiology*, *10*, 00245.

Ferrando, S., Gallus, L., Ghigliotti, L., Amaroli, A., Abbas, G., & Vacchi, M. (2017). Clarification of the terminology of the olfactory lamellae in chondrichthyes. *The Anatomical Record*, *300*(11), 2039–2045.

Gignac, P. M., Kley, N. J., Clarke, J. A., Colbert, M. W., Morhardt, A. C., Cerio, D., Cost, I. N., Cox, P. G., Daza, J. D., Early, C. M., Echols, M. S., Henkelman, R. M., Herdina, A. N., Holliday, C. M., Li, Z., Mahlow, K., Merchant, S., Müller, J., Orsbon, C. P., … Witmer, L. M. (2016). Diffusible iodine-based contrast-enhanced computed tomography (diceCT): An emerging tool for rapid, high-resolution, 3-D imaging of metazoan soft tissues. *Journal of Anatomy*, *228*, 889–909.

Grigg, G. C. (1970). Water flow through the gills of Port Jackson sharks. *Journal of Experimental Biology*, *52*, 565–568.

Hansen, A., & Zielinski, B. S. (2005). Diversity in the olfactory epithelium of bony fishes: Development, lamellar arrangement, sensory neuron cell types and transduction components. *Journal of Neurocytology*, *34*, 183–208.

Hara, T. (1975). Olfaction in fish. *Progress in neurobiology*, *5*(4), 271–335.

Irschick, D. J., Fu, A., Lauder, G., Wilga, C., Kuo, C.-Y., & Hammerschlag, N. (2017). A comparative morphological analysis of body and fin shape for eight shark species. *Biological Journal of the Linnean Society*, *122*(3), 589–604.

Irschick, D. J., & Hammerschlag, N. (2015). Morphological scaling of body form in four shark species differing in ecology and life history. *Biological Journal of the Linnean Society*, *114*, 126–135.

Kajiura, S. M., Forni, J. B., & Summers, A. P. (2005). Olfactory morphology of carcharhinid and sphyrnid sharks: Does the cephalofoil confer a sensory advantage? *Journal of Morphology*, *264*(3), 253–263.

Kleerekoper. (1969). *Olfaction in fishes*. Indiana University Press.

Last, P. R., & Stevens, J. D. (2009). *Sharks and rays of Australia* (2nd ed.). Hardvard University Press.

Lever, J., Krzywinski, M., & Altman, N. (2017). Principal component analysis. *Nature Methods*, *14*(14), 641–642.

Maisey, J. G. (1984). Chondrichthyan phylogeny: A look at the evidence. *Journal of Vertebrate Paleontology*, *4*, 359–371.

Meredith, T. L., Caprio, J., & Kajiura, S. M. (2012). Sensitivity and specificity of the olfactory epithelia of two elasmobranch species to bile salts. *Journal ofExperimental Biology*, *215*, 2660–2667.

Meredith, T. L., & Kajiura, S. M. (2010). Olfactory morphology and physiology of elasmobranchs. *Journal of Experimental Biology*, *213*, 3449–3456.

Naylor, G. J. P., Caira, J. N., Jensen, K., Rosana, K. A. M., Straube, N., & Lakner, C. (2012). Elasmobranch phylogeny: A mitochondrial estimate based on 595 species. In J. C. Carrier, J. A. Musick, & M. R. Heithaus (Eds.), *Biology of sharks and their relatives* (2nd ed., pp. 31–56). CRC Press.

Nelson, J. S. (2004). *Fishes of the world* (4th ed.). John Wiley & Sons, Inc.

Northcutt, R. G. (1978). Brain organization in the cartilaginous fishes. In E. S. Hodgson, & R. F. Mathewson (Eds.), *Sensory biology of sharks, skates, and rays* (pp. 117–194). Office of Naval Research.

Park, K., Kim, W., & Kim, H. Y. (2014). Optimal lamellar arrangement in fish gills. *Proceedings of the National Academy of Sciences*, *111*(22), 8067–8070.

Pashchenko, N. I., & Kasumyan, A. O. (2017). Development of the olfactory organ in the ontogeny of carps (Cyprinidae). *Journal of Ichthyology*, *57*, 136–151.

Polly, P. D., Lawing, A. M., Fabre, A.-C., & Goswami, A. (2012). Phylogenetic principal components analysis and geometric morphometrics. *Hystrix, the Italian Journal of Mammalogy*, *24*(1), 1–9.

Revell, L. J. (2009). Size-correction and principal components for interspecific comparative studies. *Evolution*, *63*, 3258–3268.

Revell, L. J. (2012). phytools: An R package for phylogenetic comparative biology (and other things): Phytools: R package. *Methods in Ecology and Evolution*, *3*, 217–223.

Rygg, A. D., Cox, J. P. L., Abel, R., Webb, A. G., Smith, N. B., & Craven, B. A. (2013). A computational study of the hydrodynamics in the nasal region of a hammerhead shark (*Sphyrna tudes*): Implications for olfaction. *PLoS One*, *8*, e59783.

Schluessel, V., Bennett, M. B., Bleckmann, H., Blomberg, S., & Collin, S. P. (2008). Morphometric and ultrastructural comparison of the olfactory system in elasmobranchs: The significance of structure-function relationships based on phylogeny and ecology. *Journal of Morphology*, *269*(11), 1365–1386.

Schluessel, V., Bennett, M. B., Bleckmann, H., & Collin, S. P. (2010). The role of olfaction throughout juvenile development: Functional adaptations in Elasmobranchs. *Journal of Morphology*, *271*(4), 451–461.

Shirai, S. (1996). Phylogenetic interrelationships of neoselachians (Chondrichthyes: Euselachii), *Interrelationships of fishes* (Vol. 2, pp. 9–34).

Strother, J. A. (2013a). Hydrodynamic resistance and flow patterns in the gills of A tilapine fish. *Journal of Experimental Biology*, *216*(14), 2595–2606.

Strother, J. A. (2013b). A computational model of flow between the microscale respiratory structures of fish gills. *Journal of Theoretical Biology*, *338*, 23–40.

Taeger, D., & Kuhnt, S. (2014). *Statistical hypothesis testing with SAS and R*. John Wiley & Sons, Incorporated.

Theisen, B., Zeiske, E., & Breucker, H. (1986). Functional morphology of the olfactory organs in the spiny dogfish (*Squalus acanthias* L.) and the small-spotted catshark (*Scyliorhinus canicula* (L.)). *Acta Zoologica*, *67*, 73–86.

Theiss, S. M., Hart, N. S., & Collin, S. P. (2009). Morphological indicators of olfactory capability in wobbegong sharks (Orectolobidae, Elasmobranchii). *Brain, Behavior and Evolution*, *73*(2), 91–101.

Timm, L. L., & Fish, F. E. (2012). A comparative morphological study of head shape and olfactory cavities of sharks inhabiting benthic and coastal/pelagic environments. *Journal of Experimental Marine Biology and Ecology*, *414–415*, 75–84.

Tricas, T. C., Kajiura, S. M., & Summers, A. P. (2009). Response of the hammerhead shark olfactory epithelium to amino acid stimuli. *Journal of Comparative Physiology A: Neuroethology, Sensory, Neural, and Behavioral Physiology*, *195*, 947–954.

Vogel, S. (2013). *Comparative biomechanics: Life's physical world* (2nd ed., p. 233). Princeton University Press.

Yamamoto, M. (1982). Comparative morphology of the peripheral olfactory organ in teleosts, *Chemoreception in Fishes* (pp. 39–59). Elsevier Scientific Publishing Company.

Yopak, K. E., Lisney, T. J., & Collin, S. P. (2015). Not all sharks are "swimming noses": Variation in olfactory bulb size in cartilaginous fishes. *Brain Structure and Function*, *220*, 1127–1143.

Zeiske, E., Theisen, B., & Gruber, S. H. (1987). Functional morphology of the olfactory organ of two carcharhinid shark species. *Canadian Journal of Zoology*, *65*, 2406–2412.

How to cite this article: Clark, A., Porter, M., & Meredith, T. (2022). Morphometric analysis of the elasmobranch olfactory rosette. *Journal of Morphology*, 1–14. https://doi.org/10.1002/jmor.21514